CHARGE ACCUMULATION AND ION FOCUSING FOR DIELECTRICS EXPOSED TO ELECTRON AND ION BEAMS

Gordon McKeil and Keith G. Balmain
Department of Electrical Engineering
University of Toronto
Toronto, Ontario, Canada, M5S 1A4

Abstract

Numerical simulations are reported which successfully reproduce the experimentally observed properties of surface charge accumulation on spacecraft dielectrics exposed to a moderate energy electron beam (20 keV) and low energy positive ions. The ions focus to produce strong differential charging with a sharply defined region of ion neutralization of the dominant negative electron charge. The properties of this "ion spot" vary with ion beam energy, current density, and beam size. The strong peaking of the surface charge at the edge of the ion spot is investigated. The electron and ion currents at the surface are obtained by calculating the particle trajectories in the electrostatic fields of the charged surface and the metal sample mounting components. Two approaches for solving these fields are attempted and discussed, a boundary charge method and a finite-element method.

Introduction

Spacecraft dielectrics, such as thermal blankets and solar panels, accumulate charge when exposed to the ambient charged particle environment. The exposed dielectrics become negatively charged because typically the electron flux is higher and more energetic than the ion flux. As a first approximation to space conditions, materials and components are often tested in the laboratory by exposing them to electron beams alone. The positive ions could be important, however, because they would be strongly attracted by

This work was supported by U.S. Air Force Weapons Laboratory and the Computer Sciences Corporation (both in Albuquerque, NM), by the Natural Sciences and Engineering Research Council of Canada, and by the Ontario Institute for Space and Terrestrial Science.
Paper presented at the Spacecraft Charging Technology Conference, held at the Naval Postgraduate School, Monterey, Calif., 31 October - 3 November 1989.

surfaces that are at high negative potential either as the result of buildup of electron charge or due to biasing (as with large solar panels).

To investigate the effects of positive ions during charging, laboratory experiments were conducted [*Gossland and Balmain*, 1983; *Balmain et al.*, 1985] in which samples of polymer sheet were exposed simultaneously to a moderate energy electron beam (typically 20 keV) and low energy ions (< 1 keV). Subsequently, numerical simulations of this electron-ion charging process were undertaken, the results of which are presented in this paper.

The experimental arrangement is depicted in Figure 1. A sample of dielectric sheet with a typical thickness of 100 μm was laid over a grounded metal substrate and covered with a grounded metal mask, thickness 1 or 2 mm, having a circular aperture with diameters from 5 mm to 50 mm. When the electron beam was initially turned on, the entire sample luminesced due to energetic electron impact with the surface. With continued exposure, the luminescence diminished as the surface acquired a negative potential which retarded the incoming electrons. When the ion source was included, a central luminescent spot which did not fade was seen. This spot is interpreted as a region of ion neutralization of the accumulated electron charge, which allowed the incoming electrons to strike the surface with most of their beam energy, causing the strong luminescence. The luminescent spot had sharp boundaries and expanded with increased ion current. Subsequent arc discharges tended to avoid the region of the spot.

Thus the positive ion charge did not distribute uniformly, resulting in some general reduction of the negative charge buildup, but concentrated in an isolated region producing strong differential charging. Other investigators [*McCoy and Konradi*, 1978] have reported similar luminescence patterns during charging of solar arrays with high negative bias in a plasma.

Surface Current Calculations through Trajectory Mapping

To study the focussing of ions theoretically, it is useful to examine the trajectories of ions approaching a negative charge distribution. Such a charge model with the resultant ion trajectories is shown in Figure 2. The ions can be seen to concentrate strongly at the center of the sample. From such trajectories, the ion current at the sample surface may be calculated [*McNeil and Balmain*, 1986] for a particular surface charge distribution.

To follow the time development of the surface charge accumulation, a simple "quasi static" approach is taken. A set of trajectories is calculated for the electrons and the ions in the electrostatic fields due to the accumulated charge on the dielectric surface up to that point in time. The charged-particle currents incident on the dielectric surface are calculated from these trajectories. From the impact velocities and angles, the secondary emission coefficients are calculated and used to obtain the net currents and associated charges deposited. These currents are held constant for a time step, accumulating more charge on the surface. A new set of trajectories is then calculated for the updated charge configuration, and the process is repeated. In this way, the charge on the sample surface is stepped through time and its evolution followed.

To describe the secondary emission and backscattering for electron bombardment, the following expression was used [*Wall et al.*, 1977]

$$SE + BS = K \times E^{0.725} \times e^{(2(1-\cos\theta))} + (0.1 \times E^{0.2})^{\cos\theta}$$

where:

E = impact energy in keV
θ = impact angle of incidence
K = a constant (0.847 for Mylar)

For polymers, the secondary electron emission coefficients due to ion bombardment are not well reported in the literature. For other materials, the values range from SE≈1 for metals and semiconductors, to SE≈10 for inorganic dielectrics [*Krebs*, 1983]. In these simulations, the following simple estimate was used.

$$SE = 0.4 \times E^{1/2}$$

Most of the computer time is consumed evaluating the electrostatic fields for the trajectory calculations. To increase efficiency, a solution for these fields allowing quick evaluation is required. Simulations are done here for cylindrically symmetric geometries. Two solution techniques were attempted and are discussed. They are designated as the filamentary-ring-boundary-charge model and the finite-element field solution.

Filamentary-Ring Boundary-Charge Model

In this model, the charge distribution on the sample surface and the surrounding grounded mask is represented by filamentary rings of charge, as shown in Figure 3. Typically fifty to one hundred rings are used to represent the sample and about twenty rings are used for the mask edge.

This approach seems to work well for early charging. However, as the surface charge increases, anomalous ion trajectories with unstable and erratic behavior are seen. Figure 4 shows an example of this, where two of the ion trajectories "skip" across the sample surface. The close-up view shows that the positive ions approach negatively charged regions of the surface and are repelled away instead of being attracted as is physically expected. The reason for this is that the field solution provided by the filamentary charge model is inadequate. Figure 5 shows the solution for the electric field normal to a negatively charged surface over a ground plane. We see that, close to the charged surface, the normal field is not uniformly attractive but oscillates between attractive and repulsive. To attempt to overcome this by increasing the number of charge filaments or by replacing the filaments with a smoother boundary-charge representation, such as with piecewise continuous sections or polynomials, would result in prohibitive computational requirements. To evaluate the field for each charge ring, a second-order elliptic integral must be evaluated. Any smoother charge representation would require third order elliptic integrals. The boundary charge technique is judged to be not suitable for use in this simulation of charge accumulation as field evaluations very close to the boundary-charge layer (the sample surface) are required.

Finite-Element Field Solution and Simulation Results

A solution to the electrostatic field problem was obtained using triangular finite elements of cubic order [*Silvester and Konrad*, 1973]. Over two hundred elements with over eight hundred nodes are used, with smaller elements near the charged surface and mask, and larger elements farther away. Figure 6 shows equipotential lines for a uniformly charged sample. The outline of the grounded mask can be discerned. This finite-element approach eliminates the anomalous trajectories and, since the field is described by bipolynomials within each element, evaluation times are fast. The drawbacks include discontinuous electric fields at the element boundaries and difficulty in obtaining good accuracy estimates [*Zienkiewicz*, 1971].

The first results of the simulation are given in Figure 7. The accumulated surface charge density is shown in a three dimensional perspective plot as a function of time and radial position. Figure 7 shows the surface charge development for a sample of Mylar sheet 100 μm thick with a circular region 75 mm in radius exposed to a 20 keV electron beam at a current density of 1 nC/mm^2/sec and a 1 keV proton beam at 0.005 nC/mm^2/sec (5% of the electron current). Initially, the ion beam is undeflected by accumulated surface charge and covers a region with a radius of 100 mm, 4/3 as large as the exposed sample radius. The central region of the sample (at the left side of the plot) with markedly less negative charge accumulation corresponds to the ion spot. The spot edge is very sharp, as was the experimentally observed luminescence pattern.

In the simulation, the energy, current density, and size of the ion beam are varied to see the effect on the surface charge accumulation. Holding the other parameters constant and increasing the ion beam energy produces a larger, less intense ion spot, as shown in Figures 8 and 9. The region of partial ion neutralization of the negative electron charge is larger, but the intensity, the degree of charge neutralization inside the ion spot, is reduced. Varying the ion beam current, but holding the ion beam energy at 1 keV, reproduces the effect seen experimentally that the larger the ion beam current, the larger the ion spot, as shown in Figures 10 and 11. The ion spot also is more intense for larger ion currents.

Finally, Figures 12 and 13 show the effect of varying the size of the ion beam. Shown is the surface charge development for ion beams which initially, without any deflection by surface charge, cover regions of radii 50 mm, 75 mm, 100 mm, and 300 mm, or 2/3, 1, 4/3, and 4 times the radius of the exposed dielectric sample. The ion spot shrinks with reduced ion beam size, but the intensity remains roughly the same. Figure 14 shows how the ion trajectories for the widest ion beam completely envelope the sample area. Therefore, if the size of the ion beam were further increased, the additional ions would hit the grounded mask and not the dielectric sample and the surface charge accumulation or ion spot size would be unchanged.

The surface charge densities show a curious peak just at the edge of the ion spot where the charge density actually reaches positive values for some cases. Examination of the charge accumulation due to the electrons and ions separately indicates that two different mechanisms are involved in the formation of these peaks, depending on the size of the ion beam. Figure 15 shows the separate electron and ion charge distributions for the case with the ion beam having a radius equal to the sample radius. Here the spot edge peak is not due to any extreme concentration of ions as the ions only charge profile

contains no such feature. Rather, the electron and ion surface charge profiles each have abrupt changes at the spot edge which tend to cancel each other, and the spot-edge peak arises because of the relative alignment of these abrupt changes. It is not clear yet whether this is a physical or numerical effect. For the widest ion beam of four times the sample radius the peak is much broader, as Figures 12 and 13 show. Separating the surface charge due to the electrons and ions for this wide ion beam case, as shown in Figure 16, reveals that the peak is now reflected in a concentrated build up of ion charge. This ion concentration at the spot edge can been seen as well in the trajectories of Figure 14. Because of the similarity between the ions-only charge profile and the electrons-plus-ions charge profile, the edge-peak for the wide beam case is thought to be a physical, rather than purely numeric effect. Other authors have also seen strong peaking of incident ion current at the edge of a region of ion focussing [*Parker et al.*, 1983].

Conclusion

The simulation study confirms the experimental observations of strong differential charging and the formation of the ion spot when lower energy positive ions are included during electron beam charging of spacecraft dielectrics. The spot characteristics have been shown to depend on the parameters of the ion beam, that is the beam energy, current and size. The boundary-charge model used to describe the accumulated surface charge is inaccurate when calculating trajectories of lower energy particles which closely approach the charged surface. The finite-element approach is a more accurate alternative. In general, it is observed that ion focussing strongly affects the currents incident at the surface of exposed materials and therefore should be considered in the design of systems where charge accumulation or particle bombardment are of concern.

References

Balmain, K. G., A. Battagin, and G. R. Dubois, Thickness scaling for arc discharges on electron-beam-charged dielectrics, *IEEE Trans. Nucl. Sci., NS–32*(6), 4073–4078, 1985.

Gossland, M., and K. G. Balmain, Incident ion effects on polymer surface discharges, *IEEE Trans. Nucl. Sci., NS–30*(6), 4302–4306, 1983.

Krebs, K. M., Recent advances in the field of ion-induced kinetic electron emission from solids, *Vacuum, 33*(9), 555–563, 1983.

McCoy, J. E., and A. Konradi, Sheath effects on a 10 meter high voltage panel in simulated low earth orbit plasma, in *Proceeding of the Spacecraft Charging Technology Conference – 1978, NASA CP–2071, AFGL–TR–79–0082*, pp. 315–340, National Aeronautics and Space Administration, Washington, D.C., 1978. **ADA084626**

McKeil, G., and K. G. Balmain, Analysis of the ion spot phenomenon on beam-charged dielectrics, *IEEE Trans. Nucl. Sci., NS–33*(6), 1396-1401, 1986.

Parker, L.W., E. G. Holeman, and J. E. McCoy, Sheath shapes: a 3–D generalization of the Child–Langmuir sheath model for large high-voltage space structures in dense plasmas, in *Proceedings of the Air Force Geophysics Laboratory Workshop on Natural Charging of Large Space Structures in Near Earth Polar Orbit, AFGL–TR–83–0046*, edited by R. C. Sagalyn, D. E. Donatelli, and I. Michael, pp. 337–389, Air Force Geophysics Laboratory, Massachusetts 1983. **ADA134894**

Silvester P., and A. Konrad, Axisymmetric triangular finite elements for the scalar Helmholtz equation, *Int. Jour. Numer. Meth. Eng.*, 5, 481–497, 1973.

Wall, J. A., E. A. Burke, and A. R. Frederickson, Results of a literature search on dielectric properties and electron interaction phenomena related to spacecraft charging, in *Proceedings of the Spacecraft Charging Technology Conference – 1977, NASA TMS–73537*, pp. 569–592, National Aeronautics and Space Administration, Washington, D.C., 1977.

Zienkiewicz, O. C., *The Finite Element Method in Engineering Science*, McGraw Hill, New York, N.Y., 1971

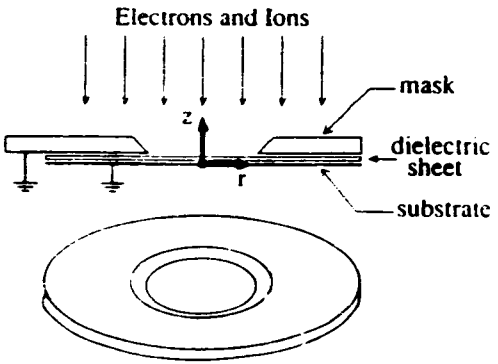

Figure 1

Schematic of experimental arrangement used to expose samples to electron and ion beams. Dielectric sheets were sandwiched between a metal substrate and a metal mask with a circular aperture. The r- and z-axes of the cylindrical coordinate system used throughout the paper are also shown.

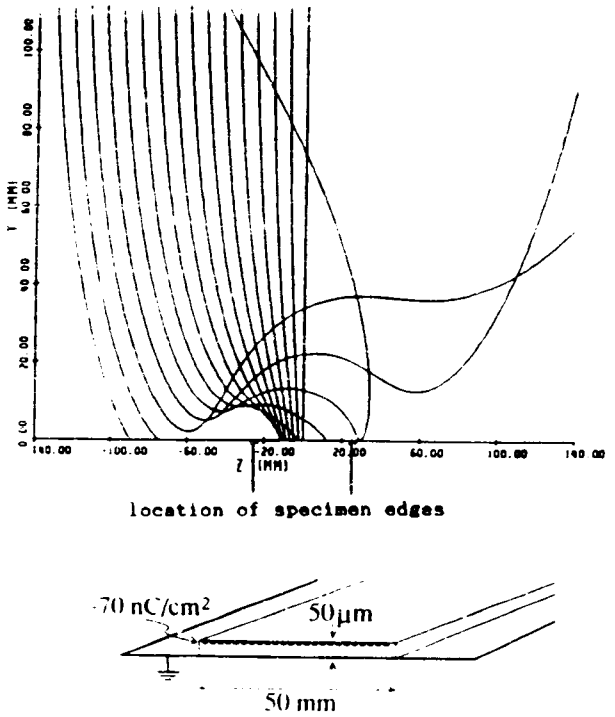

Figure 2

An example of a negative charge distribution and the ion trajectories in the resultant electrostatic field showing ion focussing towards the center.

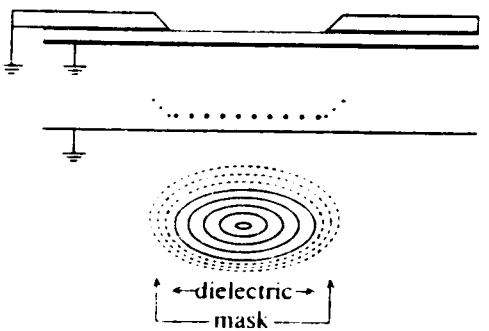

Figure 3

In the filamentary ring boundary charge model the charged dielectric sheet and the surrounding metal mask are represented by filamentary rings of charge over a ground plane, as shown.

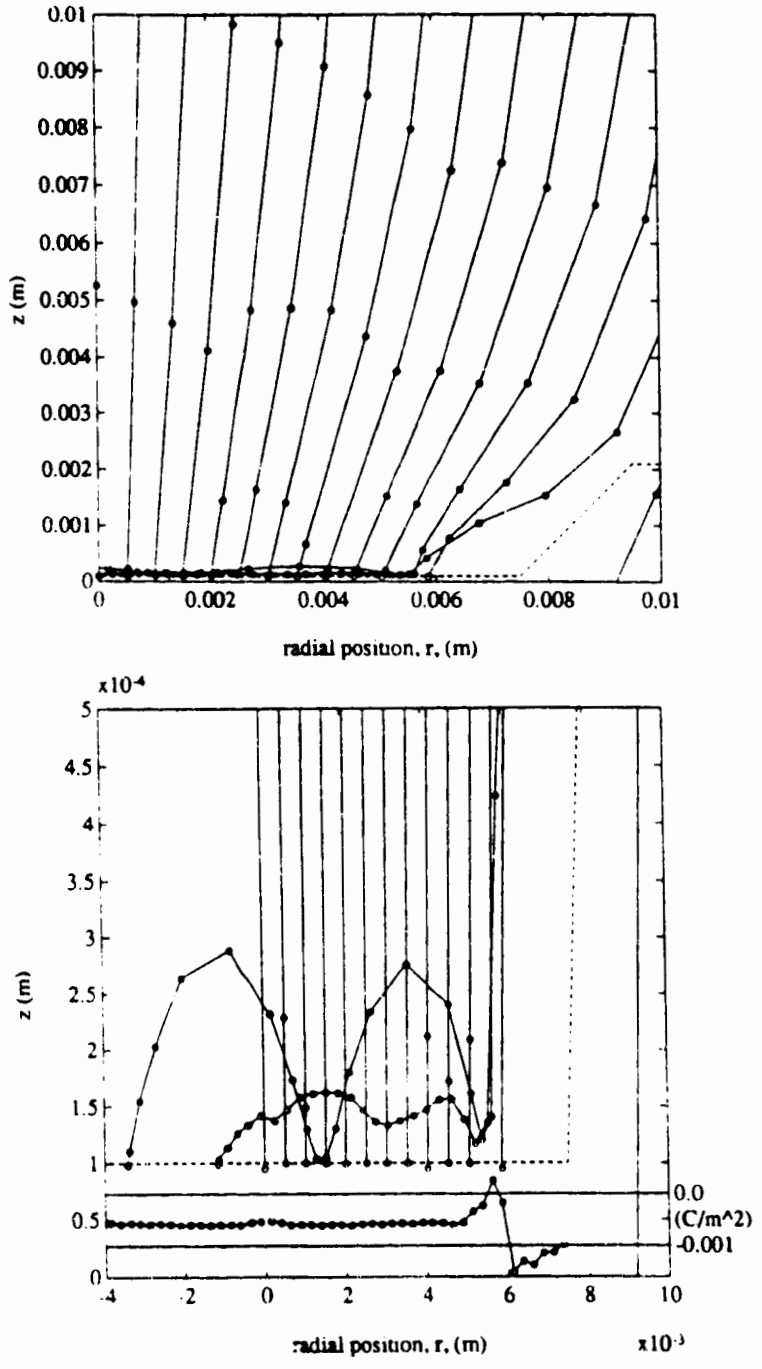

Figure 4 Anomalous trajectories for positive ions approaching a highly charged dielectric and grounded mask. The outline of the dielectric surface and mask are shown with the dashed line. The lower chart shows a close-up view with an expanded vertical distance scale given at the left. A sketch of the surface charge density is included at the bottom with its scale indicated to the right. Two of the right-most trajectories approach negatively charged regions of the surface but are repelled instead of being attracted.

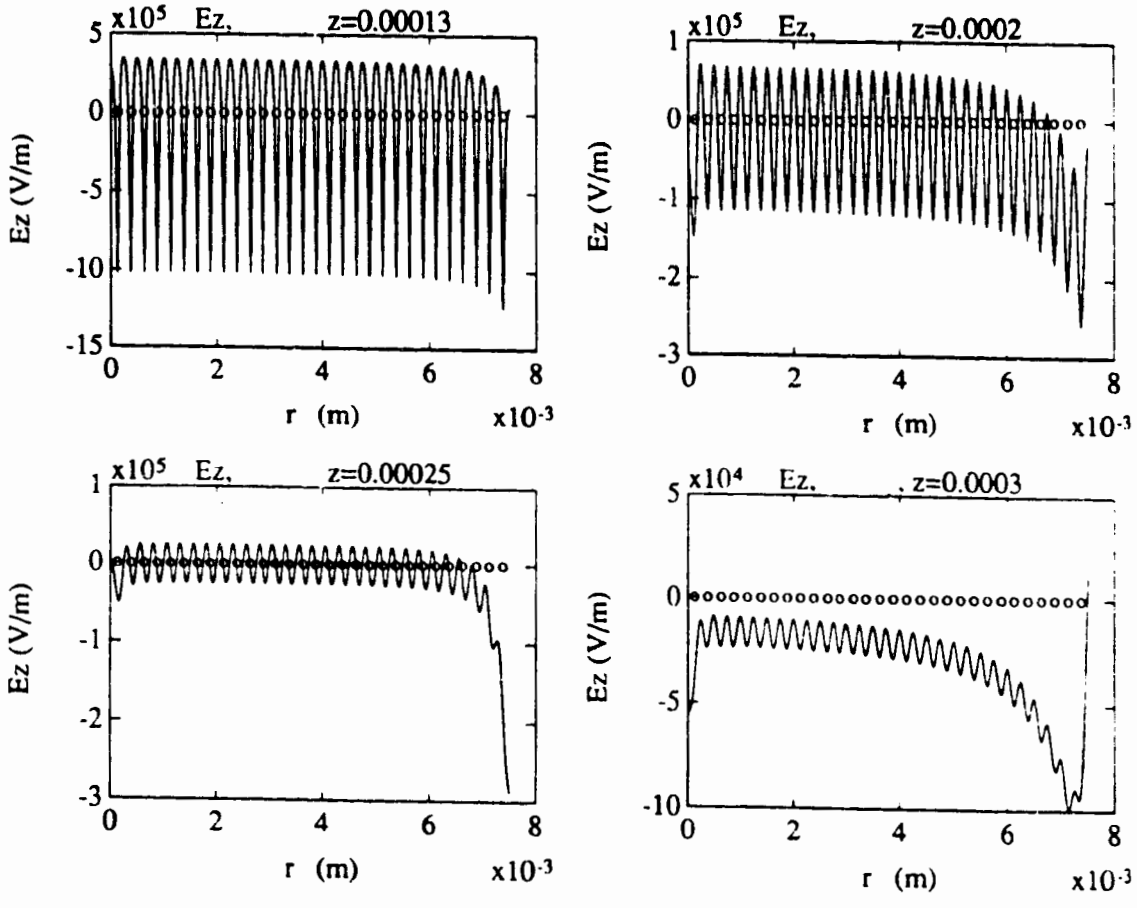

Figure 5 Solution for the normal electric field obtained using the filamentary ring boundary charge model for a dielectric sample with uniform negative surface charge density. The sample thickness is 0.0001 m and the normal field is given for positions of z= 0.00013 m, 0.0002 m, 0.00025 m, and 0.0003 m. Physically, the fields are expected to be negative, except perhaps near the mask edge, however, due to inadequacies of the model, the field oscillates wildly near the surface. The charge model and the coordinate system used are depicted in Figure 3.

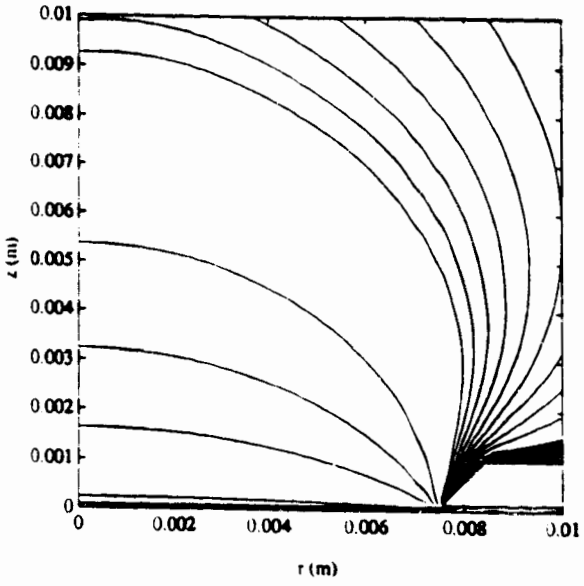

Figure 6 Equipotential lines of the finite element solution for a uniformly charged sample. The outline of the grounded mask can be discerned at the lower right.

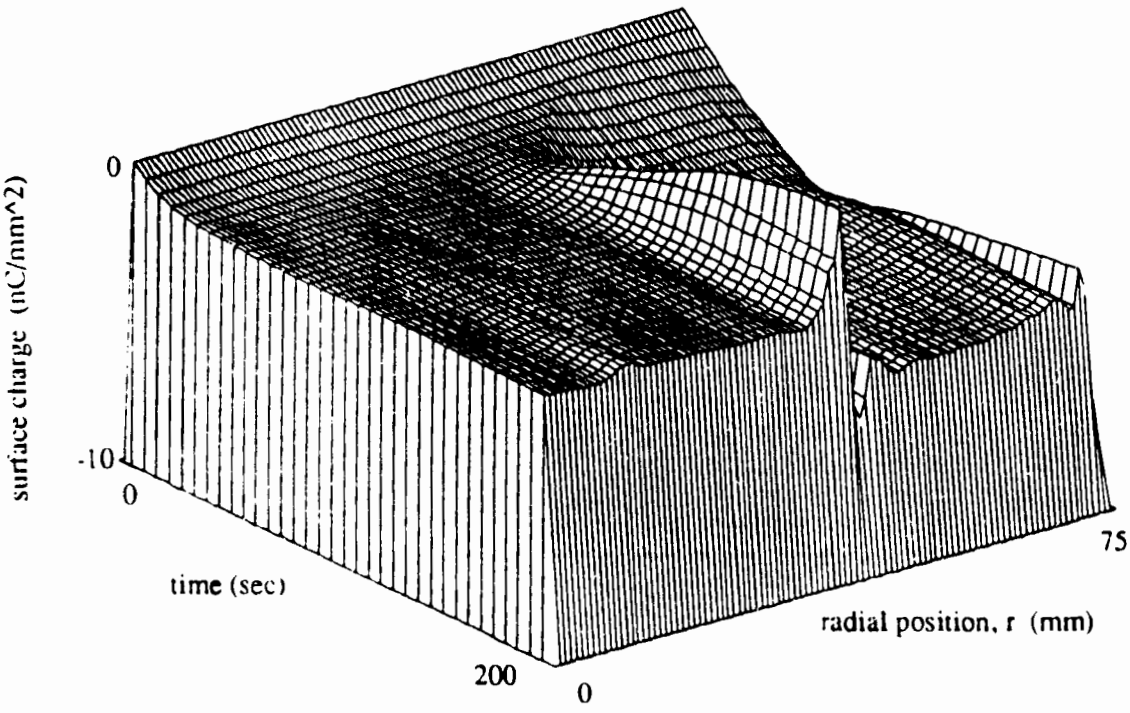

Figure 7 Developing surface charge density shown in a 3-D perspective plot as a function of time and radial position for a 100 μm thick Mylar sample with a circular region of radius 75 mm exposed to a 20 keV, 1 nC/mm^2/sec electron beam and a 1 keV, 0.005 nC/mm^2/sec proton beam which initially, before deflection by surface charge, extends to a radius of 100 mm, or 4/3 as large as the dielectric sample.

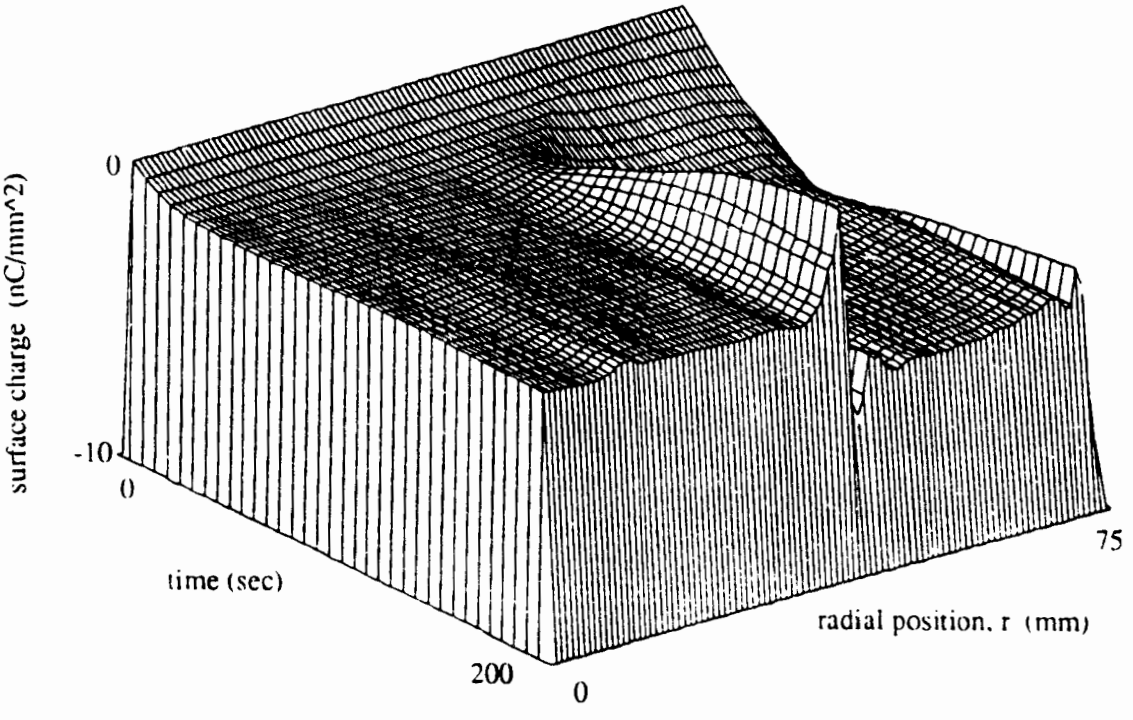

Figure 8a) Surface charge accumulation with an ion beam energy of 1 keV.

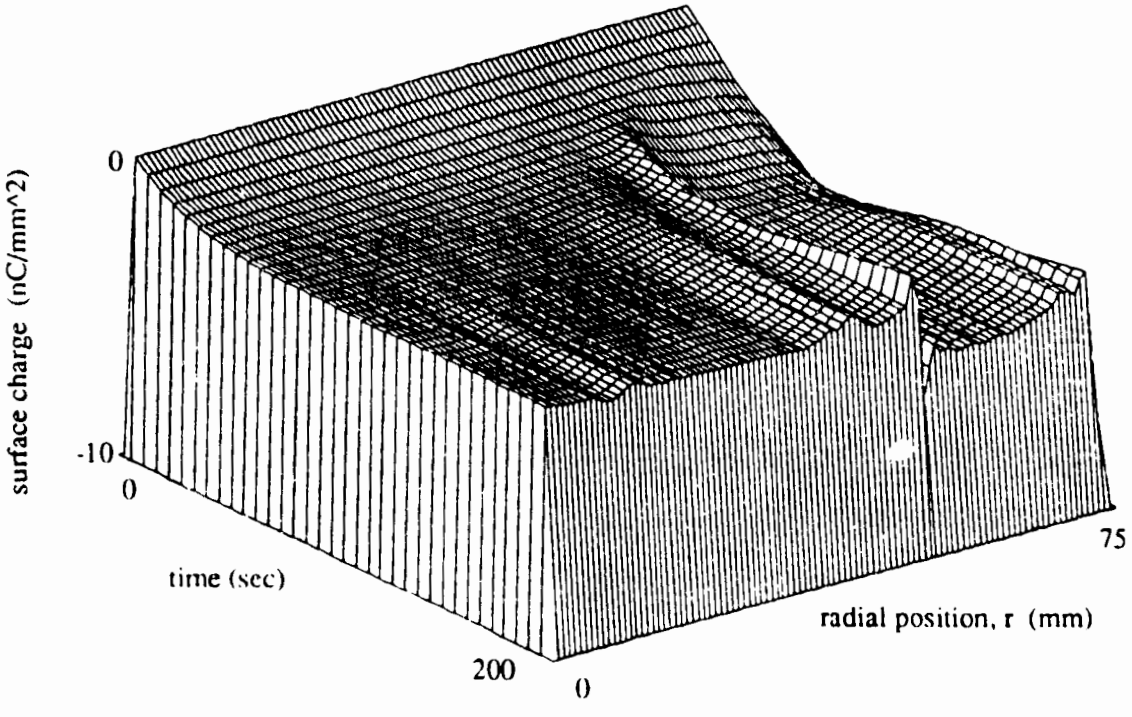

Figure 8b) Surface charge accumulation with an ion beam energy of 2 keV.

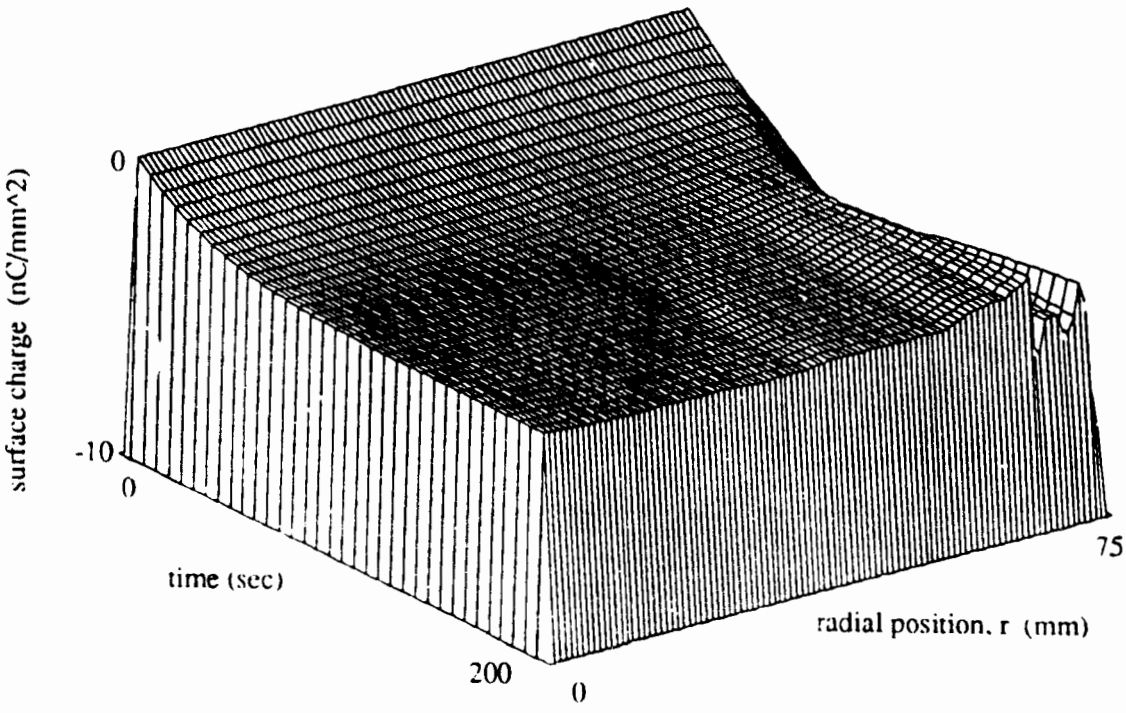

Figure 8c) Surface charge accumulation with an ion beam energy of 5 keV.

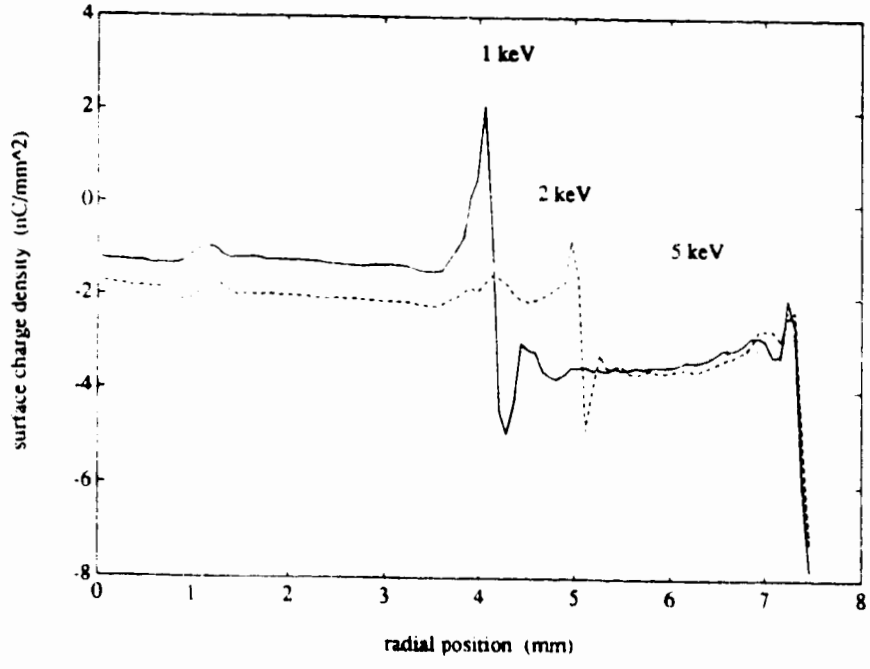

Figure 9 Ultimate surface charge accumulation on a dielectric sample exposed to ion beams of three different energies.

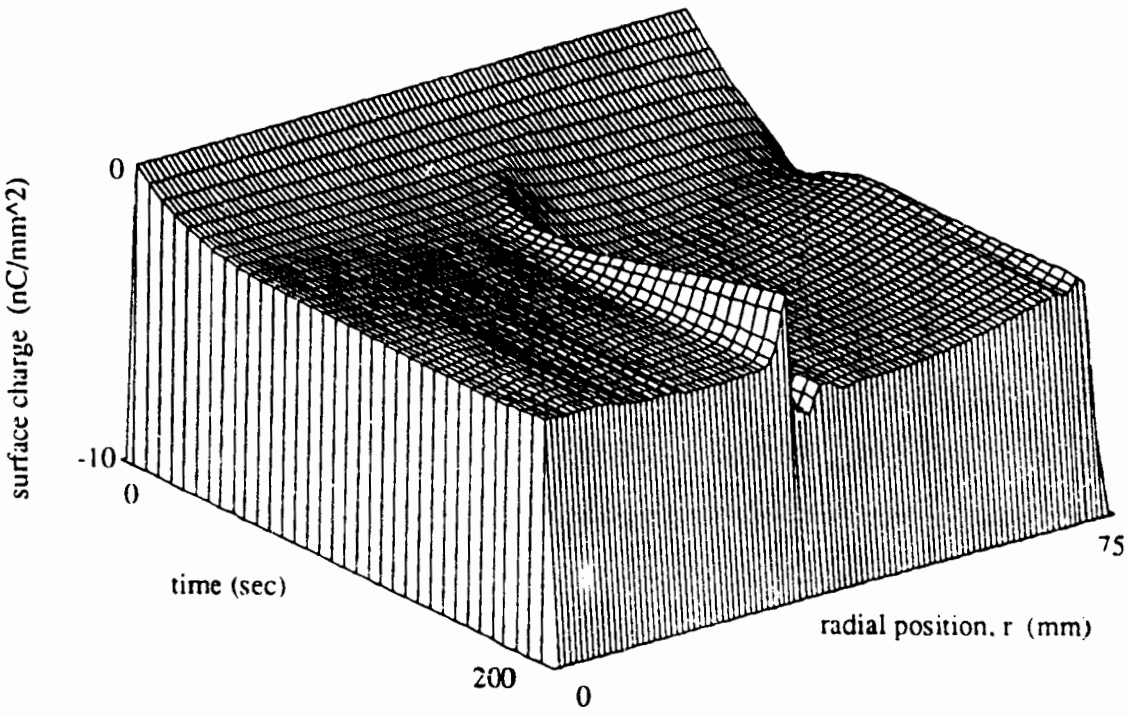

Figure 10a) Surface charge accumulation with ion beam current density of 0.002 nC/mm^2/sec, 2% the electron current density

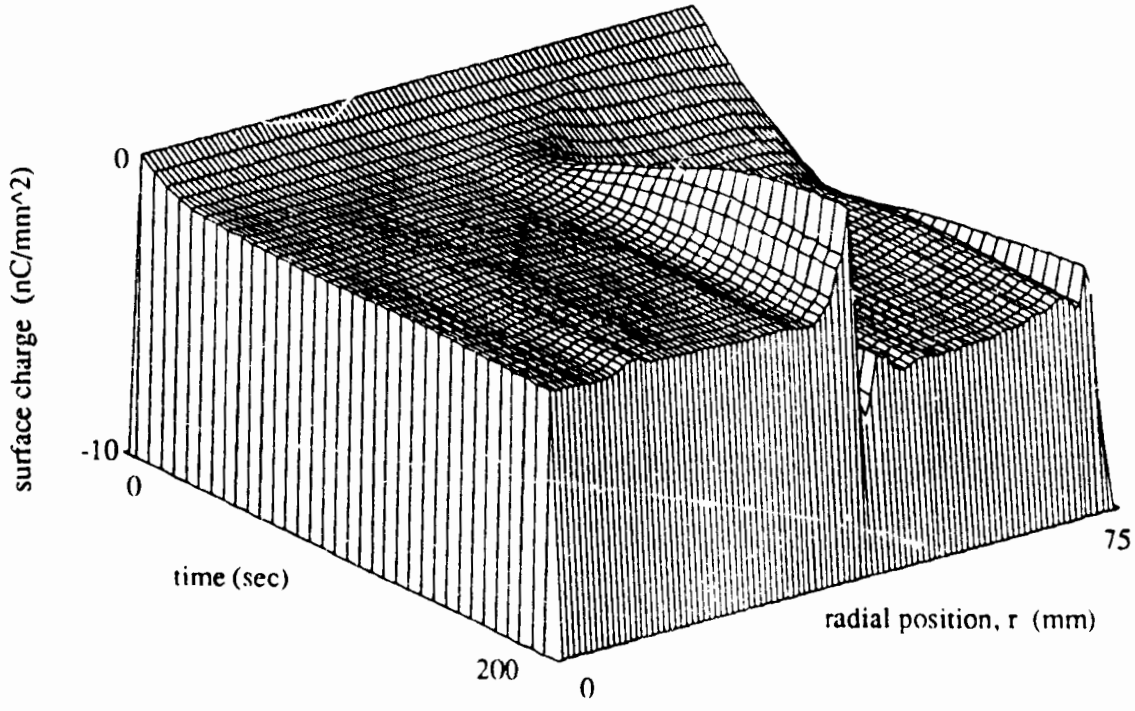

Figure 10b) Surface charge accumulation with ion beam current density of 0.005 nC/mm^2/sec, 5% the electron current density.

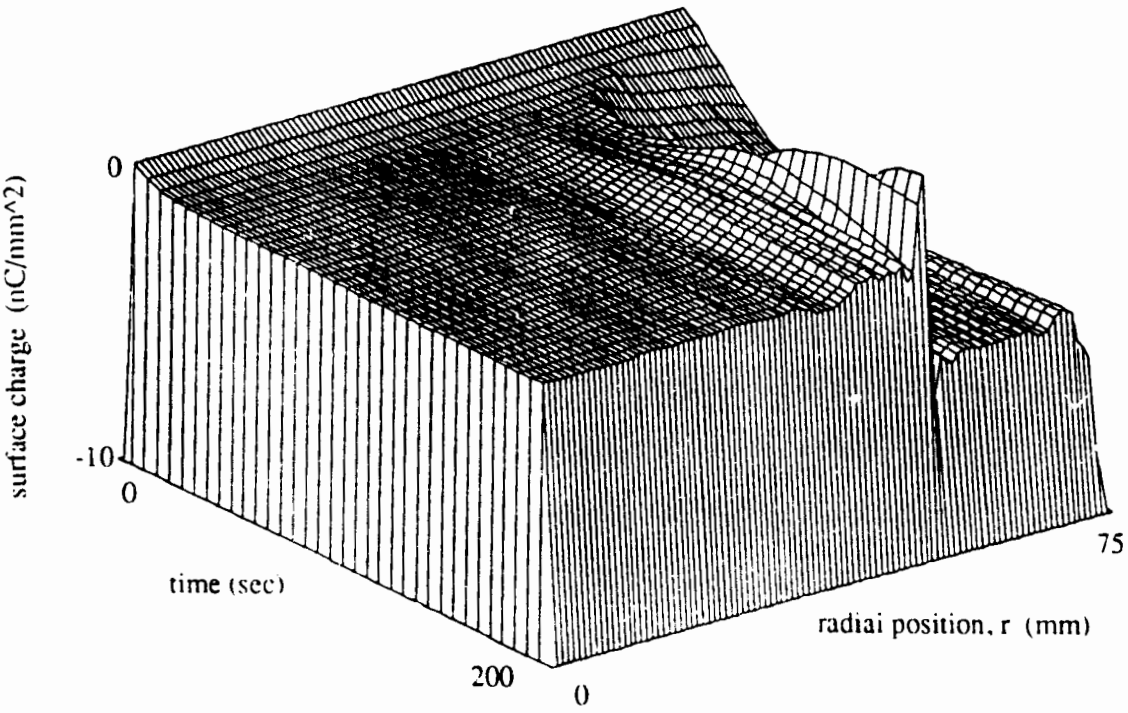

Figure 10c) Surface charge accumulation with ion beam current density of 0.010 nC/mm^2/sec, 10% the electron current density

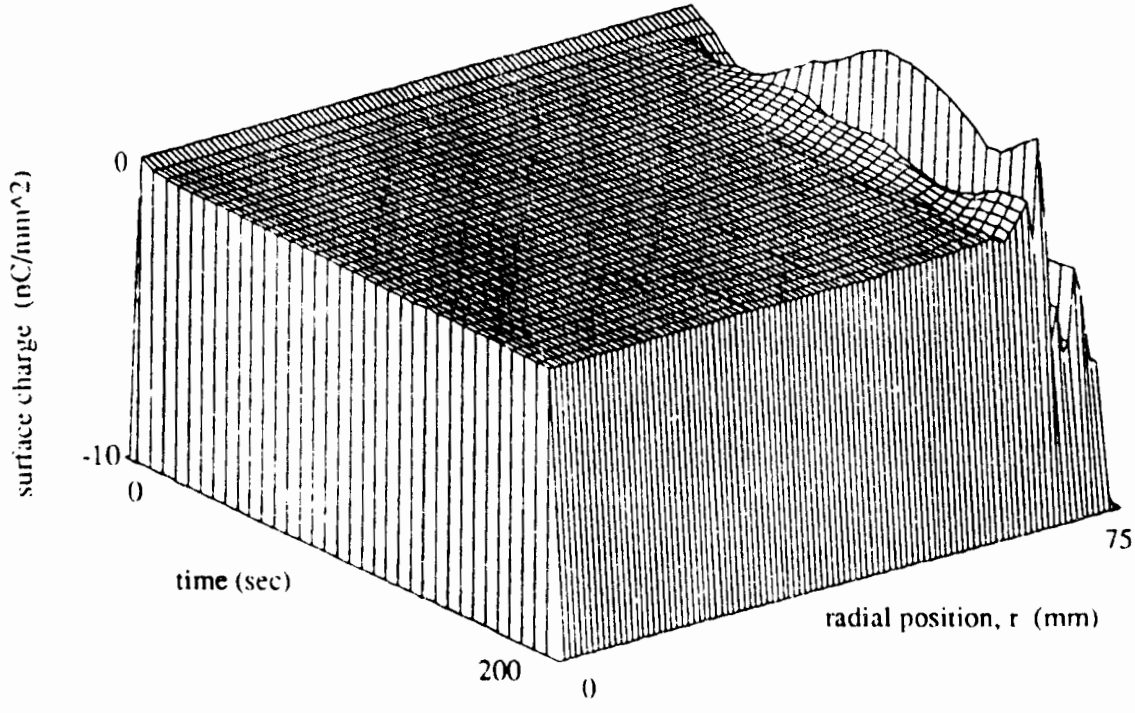

Figure 10d) Surface charge accumulation with ion beam current density of 0.020 nC/mm^2/sec, 20% the electron current density

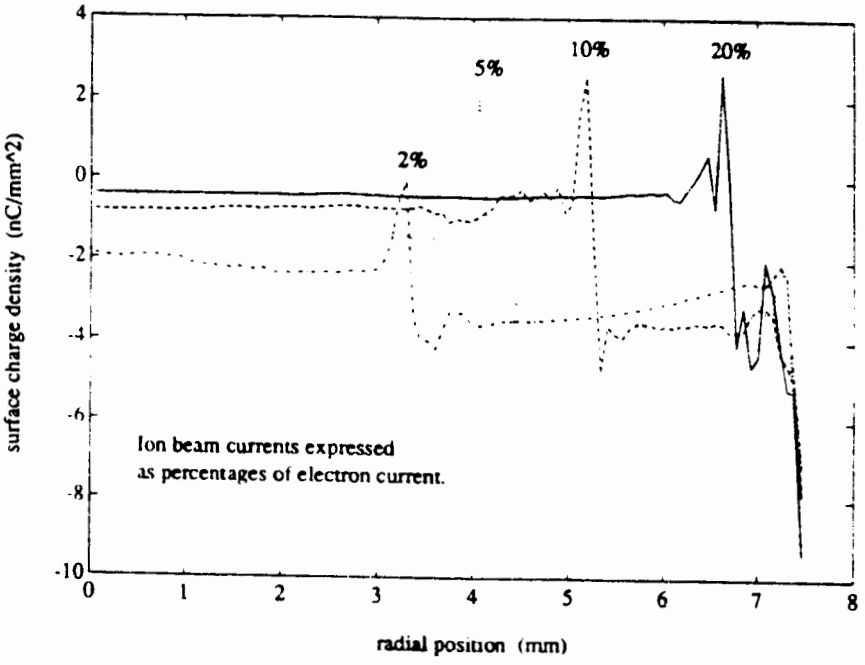

Figure 11 Ultimate surface charge accumulation on a dielectric sample exposed to ion beams of four different current densities.

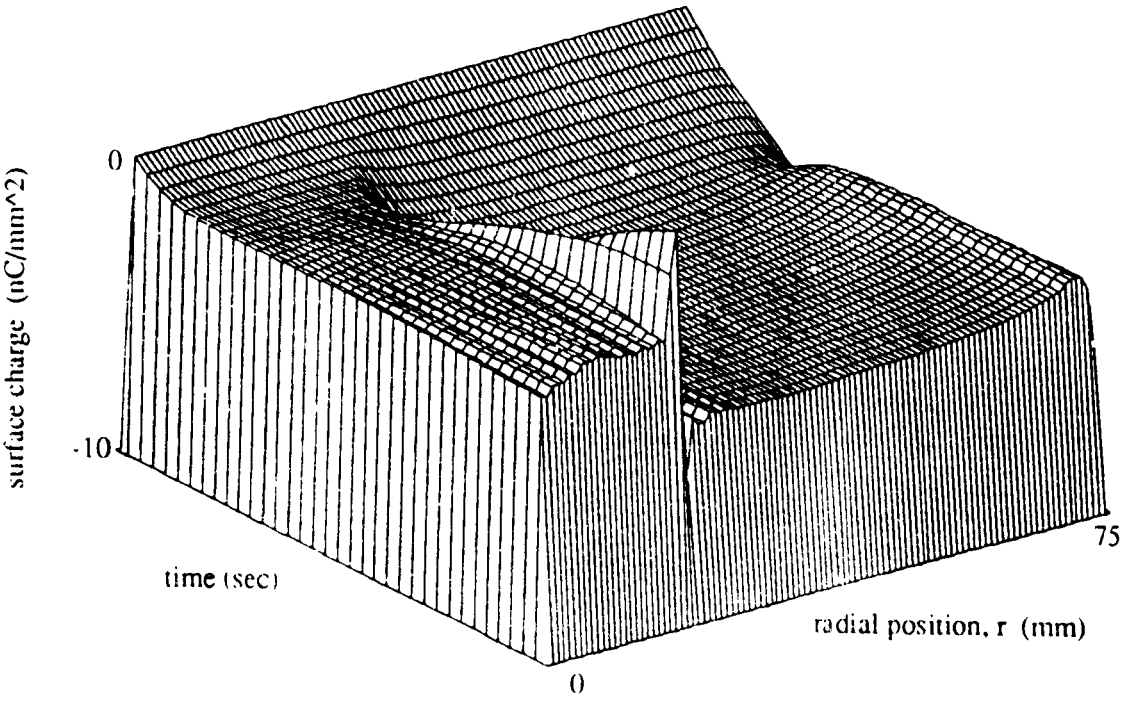

Figure 12a) Surface charge accumulation with ion beam of radius of 50 mm, 2/3 the sample radius.

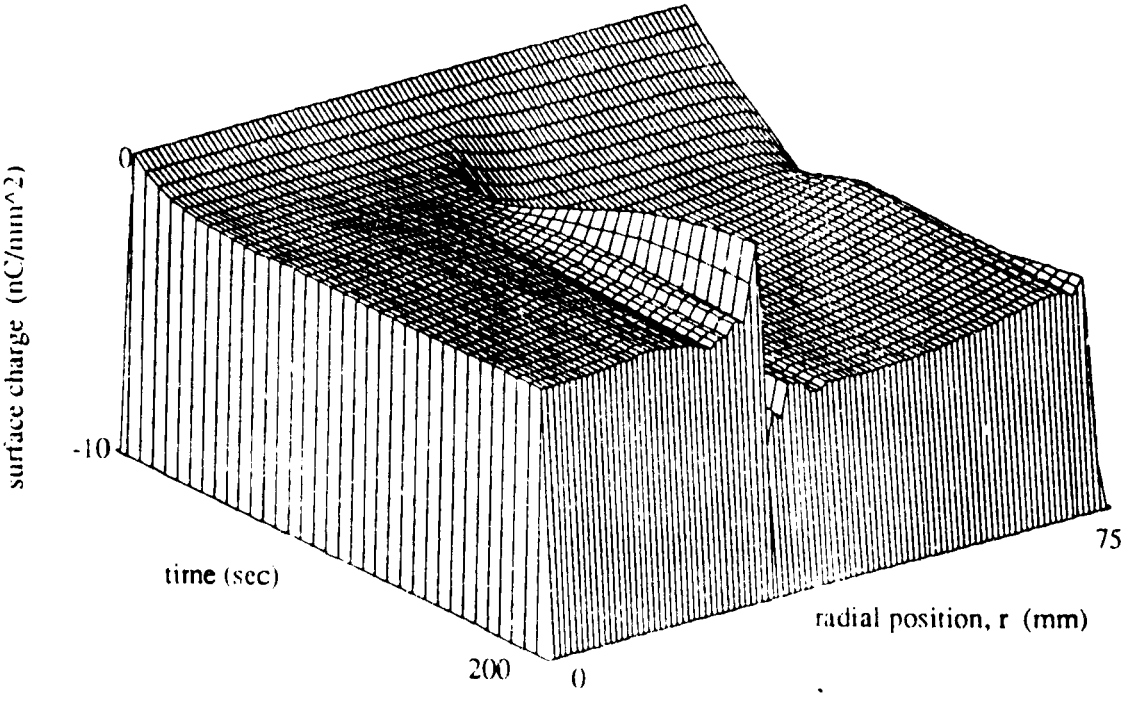

Figure 12b) Surface charge accumulation with ion beam of radius equal to sample radius.

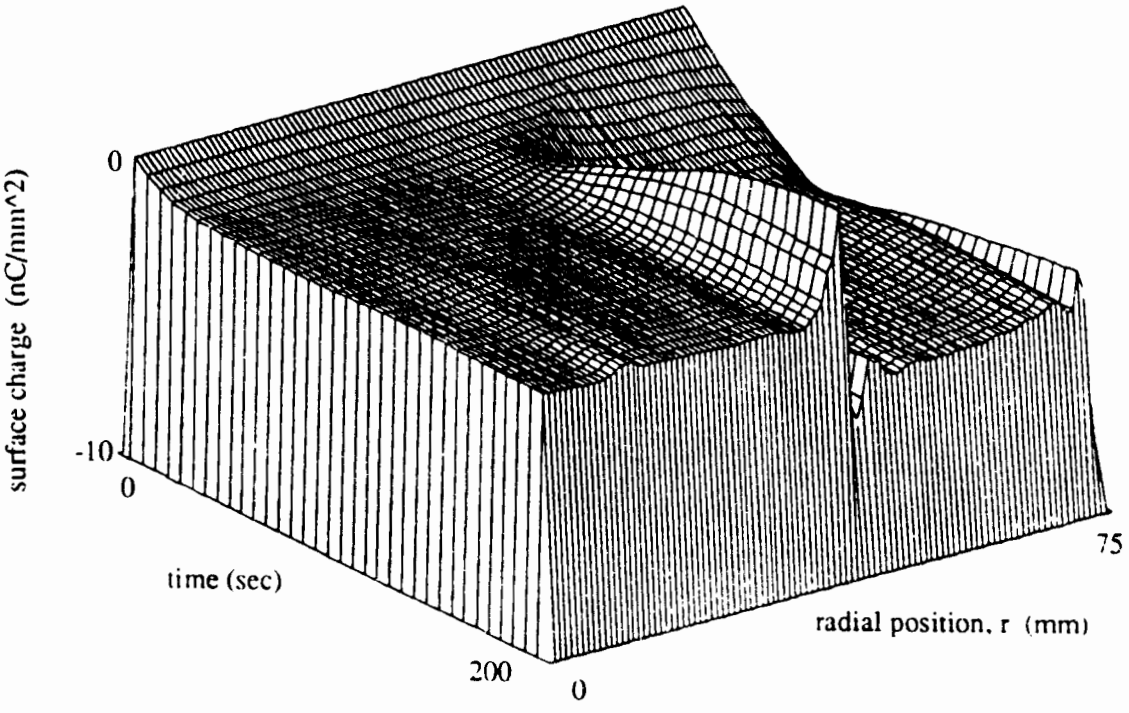

Figure 12c) Surface charge accumulation with ion beam radius of 100 mm, 4/3 the sample radius.

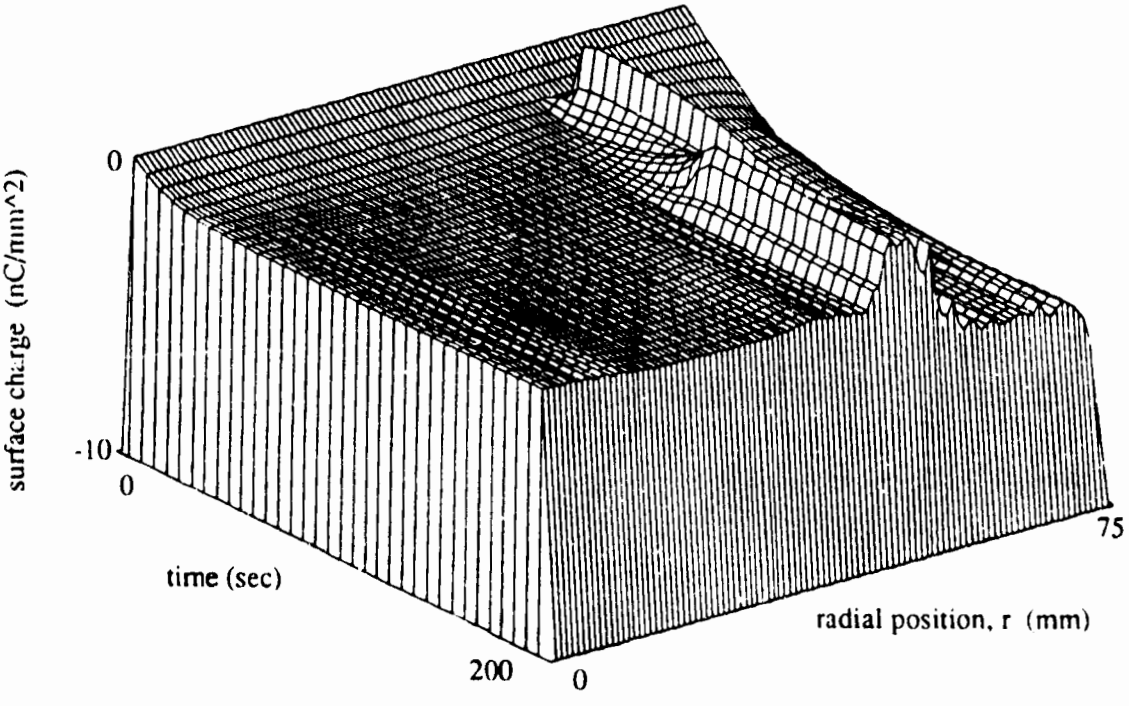

Figure 12d) Surface charge accumulation with ion beam radius of 300 mm, 4 times the sample radius.

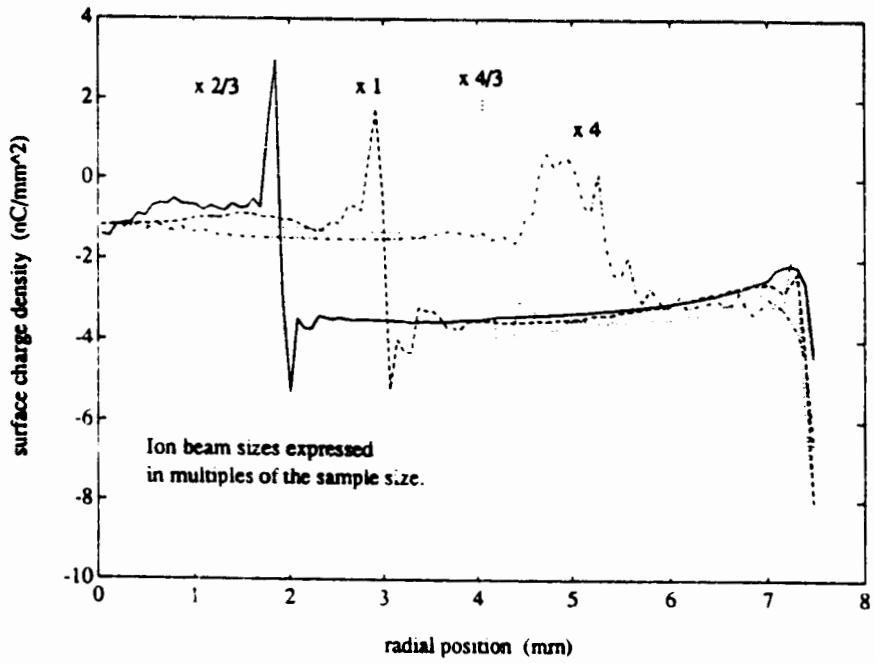

Figure 13 Ultimate surface charge accumulation on a dielectric sample exposed to ion beams of four different sizes.

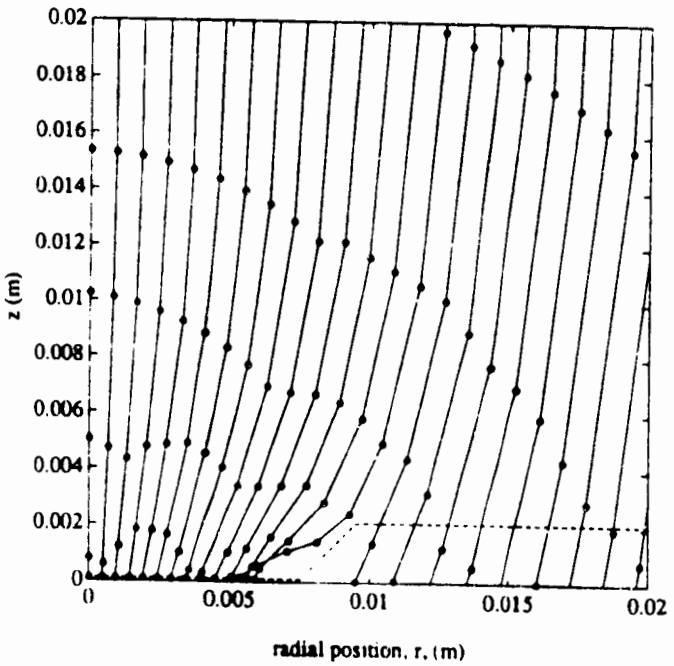

Figure 14 Ion trajectories for the ion beam with radius 4 times as large as the sample. The outline of the charge surface and the grounded mask is shown by the dashed line.

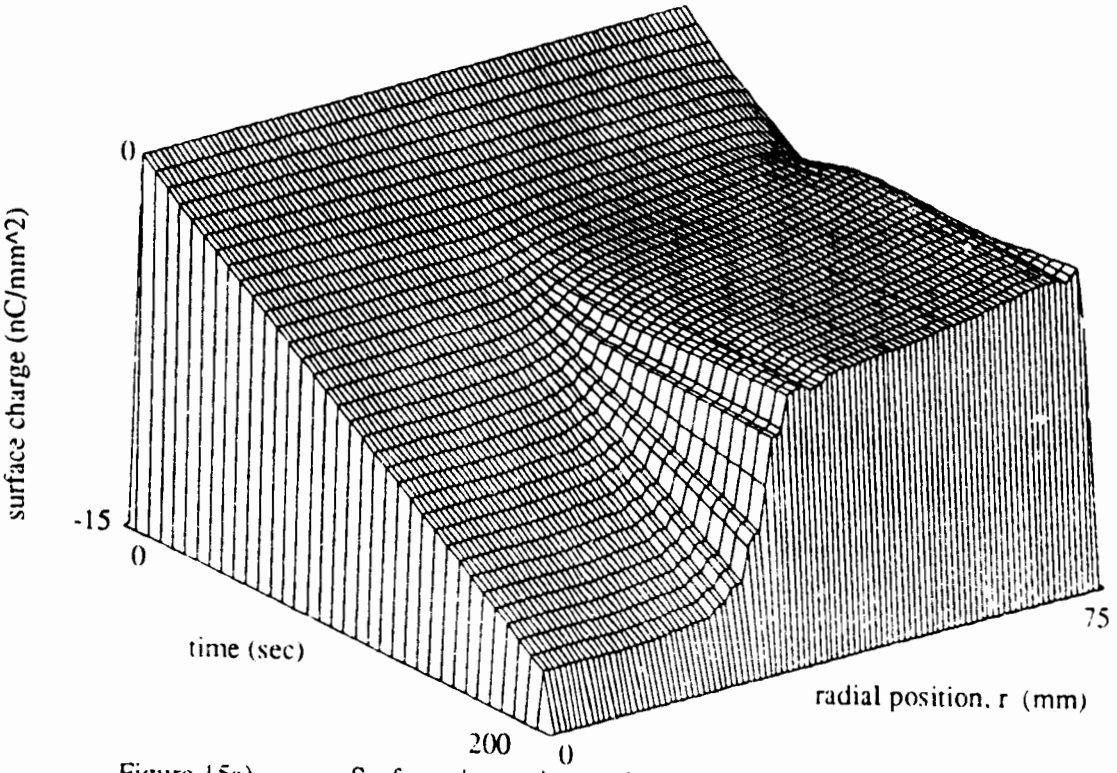

Figure 15a) Surface charge due to electrons only with ion beam of radius equal to sample radius.

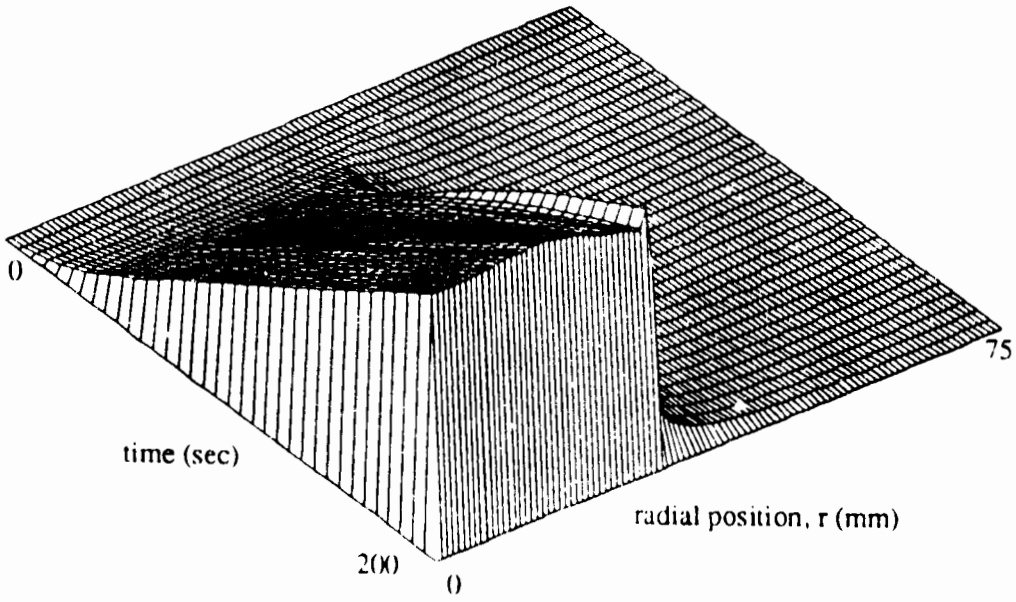

Figure 15b) Surface charge due to ions only with ion beam of radius equal to sample size.

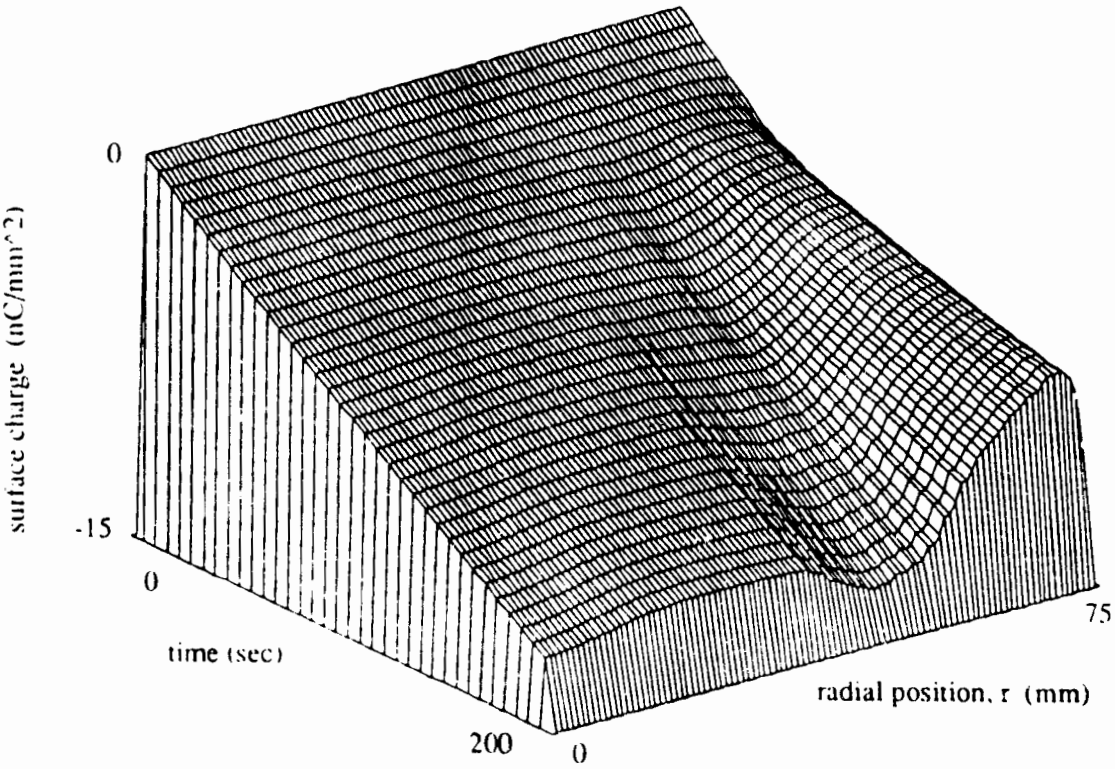

Figure 16a) Surface charge due to electrons only
for an ion beam radius of four times the sample radius.

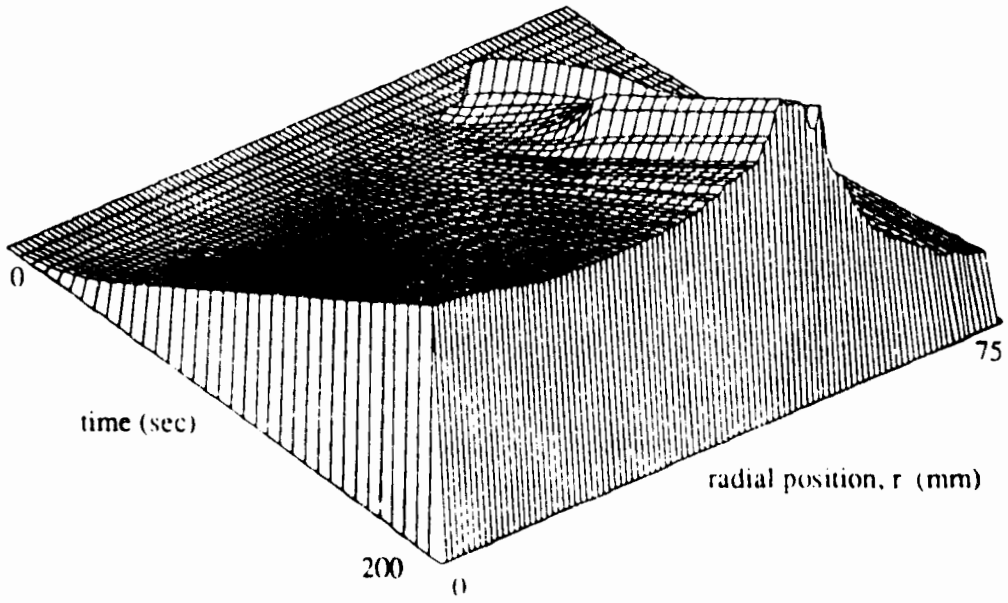

Figure 16b) Surface charge due to ions only
for an ion beam radius of four times the sample radius.